Theor Chem Acc (1997) 97:81–87

Theoretical
Chemistry Accounts

An ab initio analysis of the electronic structure and harmonic frequencies of nickel porphyrin

Mari Carmen Piqueras, Celeste McMichael Rohlfing

Cumbustion Chemistry Department, Sandia National Laboratories, Livermore, CA 94551-0969, USA

Received: 7 January 1997 / Accepted: 6 May 1997

Abstract. Ab initio calculations are performed to understand the geometry, electronic structure, and vibrational frequencies of nickel porphyrin (NiP). Hartree-Fock (HF) and second-order perturbation (MP2) theories are applied with polarized basis sets. The calculated geometrical parameters are in very good agreement with the crystal structure determination. The electronic structure and bonding are analyzed in terms of complexation and correlation effects. Not unexpectedly, the HF depiction of the metal-porphyrin interaction is rather ionic while ligand σ donation is dominant at the MP2 level. Scaled HF frequencies of NiP and its isotopomers are in very good agreement with observed infrared and resonance Raman data.

Key words: Electronic structure – Harmonic frequencies – Nickel porphyrin

1 Introduction

Ab initio quantum chemical calculations for small and medium-sized molecules generally yield accurate geometric structures and vibrational frequencies with respect to experimental results. In addition, the computed electronic structure provides qualitative insight into the bonding mechanisms. Software and hardware technologies have advanced to the point where ab initio optimized geometries and harmonic frequencies can be calculated for large transition-metal-containing molecules such as metalloporphyrins.

Metalloporphyrins consist of a macrocyclic tetrapyrrole system with a central metal atom, which may be situated in or above the mean plane of the porphyrin framework. The nature of substituents attached to the porphyrin perimeter can vary the geometric and electronic properties of the complex. Specifically, nonplanarity of the porphyrin framework is induced by steric interactions between bulky substituents, and multiple conformers are possible. The photochemical reactivity of metalloporphyrins is sensitive to the degree of nonplanarity, since excitation can result in geometrical distortions to other stable conformers. The novel conformationally dependent photophysics of nickel porphyrins in particular suggests their possible application as optoelectronic materials. Because of this potentially important use, we examine here the geometry and vibrational frequencies of the parent nickel porphyrin (NiP) (see Fig. 1), with ab initio quantum chemical methods. Our results will be used to guide future computational studies of larger nickel porphyrins.

A brief description of previous ab initio work on free-base porphyrin (H_2P) which is presumed experimentally to have a delocalized D_{2h} geometry, provides a useful background to understanding issues relevant to NiP. In the pioneering work of Almlöf et al. on H_2P [1], it was shown that Hartree-Fock (HF) theory yields a qualitatively incorrect, bond-alternating structure of C_{2v} symmetry. This is indicated by the presence of two degenerate, low-symmetry, Kekule-type geometries with alternating single and double bonds that have a lower HF energy than the high-symmetry delocalized structure. Expanding the basis set does not eliminate symmetry-breaking, but rather increases the energy separation between the localized and delocalized forms, as well as the degree of bond alteration in the localized structure. However, the overall threshold to symmetry-breaking remains low, e.g., 4.3 kcal/mol with a doubly polarized triple-zeta basis.

Inclusion of electron correlation at the levels of second-order perturbation theory (MP2) or density functional theory (DFT) yields the correct, delocalized D_{2h} structure [1]. However, the resulting stabilization energy of the D_{2h} form is quite different by these two methods. Correlation effects in H_2P were subsequently analyzed in detail by Merchan et al. [2], using complete active space self-consistent field (CASSCF) and CASSCF-based second-order perturbation (CASPT2) methods. Their results support the suitability of the MP2 approach to correlation for H_2P. The recent development of a new H_2P force field from scaled DFT force constants by

Correspondence to: M.C. Piqueras

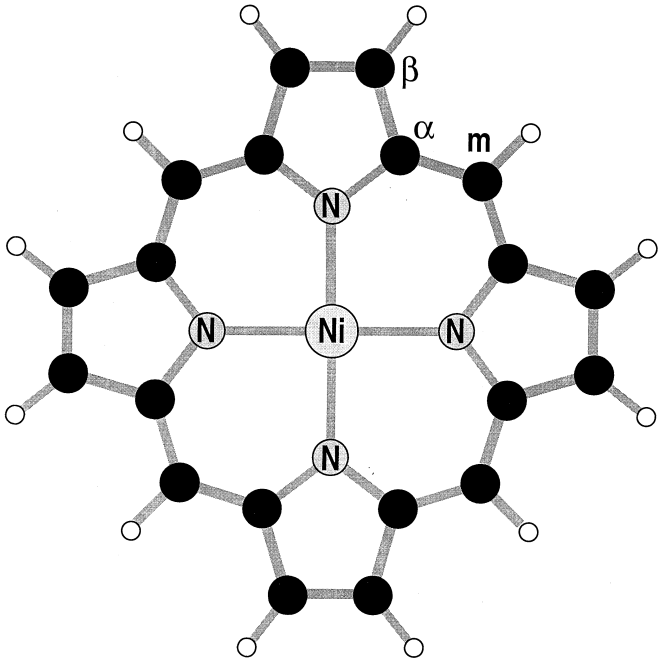

Fig. 1. Atom labeling scheme for NiP

Pulay and co-workers [3] is also noteworthy, as it is successful in reproducing experimental frequencies and intensities, and even in suggesting reassignment of some modes. Similar work is in progress for NiP [4].

We recently investigated whether the introduction of a central metal atom is a perturbation sufficient to restore symmetry to the porphyrin framework at the HF level through metal-nitrogen bonding interactions [5]. For NiP, the stable minimum at the HF level is a planar C_{2v} form, with alternating single and double bonds analogous to the HF minimum found for H_2P. The delocalized D_{4h} structure exhibits a pair of imaginary frequencies, corresponding to the expected in-plane distortions towards one or the other bond-alternating geometry. The threshold to symmetry-breaking, however, is much smaller in NiP, e.g., 0.4 kcal/mol at HF/6-311G(d). Given this lower threshold relative to H_2P, it is almost certain that the higher symmetry D_{4h} structure of NiP is the true minimum upon inclusion of electron correlation.

In this work, we investigate the performance of the HF and MP2 methods in describing the geometry, bonding, and vibrational frequencies for NiP. Although the HF treatment of NiP is limited by a slight symmetry-breaking and a nonquantitative representation of the transition metal-ligand interaction, we find that the HF D_{4h} geometry and scaled harmonic frequencies are in fact in very satisfactory agreement with experimental measurements. Our HF bonding analysis is also consistent with the empirical four-orbital model developed from spectroscopic data. Finally, we find that the inclusion of electron correlation via MP2 markedly improves the predicted geometry, although frequency evaluation at this level remains prohibitive. The success of the HF method in describing certain aspects of NiP suggests that this level of theory may be applied judiciously to nickel porphyrins with large substituent groups, which presently are not yet tractable at the MP2 level.

2 Computational methods

Figure 1 depicts the D_{4h} structure of NiP and the atom labeling convention (C_α, C_β, and C_m) used in this work. The C_m designation corresponds to meso carbons of the methine bridge while C_β corresponds to the peripheral pyrrole carbons. The x and y axes lie along the Ni—N bonds, with the z axis out of the center of the porphyrin plane. The Ni $3d$ orbitals therefore correspond to the following symmetries: $d_{z^2} = a_{1g}$, $d_{xz} = d_{yz} = d_\pi = e_g$, $d_{xy} = b_{2g}$, and $d_{x^2-y^2} = b_{1g}$.

Geometry optimizations and harmonic frequency analyses were performed at the HF level using standard 6-311G and polarized 6-311G(d) basis sets. The latter includes one d function on each C and N, and one f function on Ni. The total numbers of basis functions in our NiP calculations are thus 387 and 514 for the 6-311G and 6-311G(d) basis sets, respectively. Because of large memory and disk requirements at the MP2 level, we constructed a smaller, general basis set (GBS) for use in these calculations. It consists of 6-311G(d) for Ni, 6-31G(d) for N, C_α, and C_m, and 6-31G for C_β and all hydrogens. This GBS basis provides variational flexibility in the central porphyrin region and for the metal at the expense of the outer C_βs and hydrogens. Although a compromise, the GBS is shown below to perform as well at the HF level as the larger standard basis sets, yet it totals only 366 functions.

All results were obtained using the multiprocessing Gaussian 94 suite of programs [6] on the Cray C90 and the IBM RS6000 590 cluster at the University of Minnesota and on the SGI Power Challenges at Sandia National Laboratories. Tight thresholds for convergence and geometry optimization were employed throughout. Detailed calculational results, including optimized coordinates and second-derivative matrices, are available from the authors upon request.

3 Geometry and energetics

Table 1 lists the HF energy difference between the C_{2v} minimum and the delocalized D_{4h} stationary point, and the magnitude of the imaginary e_u frequency of the D_{4h} form, for all three basis set employed here. The threshold to HF symmetry-breaking is quite low in NiP compared to H_2P [5]; it is less than 0.4 kcal/mol for the largest basis set used here, i.e., 6-311G(d). Also, the GBS results reproduce those with the 6-311G(d) basis reasonably well at considerably less computational expense.

Table 2 lists selected optimized geometrical parameters for the D_{4h} geometry of NiP. Bond lengths calculated for the C_{2v} minimum [5] bracket the corresponding D_{4h} distances by about ± 0.003 Å at the HF/6-311G level, and by ± 0.02 Å at the HF/6-311G(d) and HF/GBS levels. Thus, as with the C_{2v}-D_{4h} energy separation above, bond alternation also increase with increasing

basis set size [5]. The C_α—N—C_α bond angle is also listed in Table 2, as for the Ni—N bond length the bond angles are characteristic markers of the porphyrin core region. Finally, Table 2 lists the results of a single-crystal X-ray diffraction study by Jentzen et al. [7]. This experiment indicates that NiP is essentially planar D_{4h}, and this conclusion is supported by both single-crystal and solution-phase resonance Raman spectral analyses [7].

The HF geometrical parameters agree with experimental data to a degree typical for this level of theory applied to transition metal compounds, the expected differences being a Ni—N distance that is too long and N—C_α distance that is too short. The HF/GBS geometry reproduces closely the HF/6-311G(d) result, with the largest deviation occurring for the C_β—C_β bond length. This is not unexpected, since the main deficiency in the GBS basis is for the atoms at the porphyrin periphery. Correlation effects, as accounted for at the MP2/GBS level, correct the HF deficiencies by decreasing the Ni—N bond length and increasing the N—C_α one. The large correlation effect on the C_β—C_β bond length is probably an artifact of the smaller basis set used on these atoms. Finally, the C_α—N—C_α angle closes down when correlation is included, as the nitrogens are pulled in closer to the metal.

The best agreement with experimental results it obtained at the MP2/GBS level for the core parameters, the Ni—N and N—C_α bond lengths and the C_α—N—C_α bond angle. Of course, the comparison is not ideal since the calculated values correspond to a gas-phase geometry, free of packing forces inherent in the crystal measurement. Note that the GBS is designed to have greater flexibility in the core region, and consequently the MP2-optimized value for the perimeter C_β—C_β bonds is poorest in comparison.

Optimized geometries are also reported for the porphyrin dianion, P^{-2} (Table 2) to illustrate the porphyrin framework reorganization upon the addition of a central Ni. The bonding interaction between Ni and N, discussed in more detail below, results in a contraction of the P^{-2} core, with a concomitant decrease in the C_α—N—C_α angle. The N—C_α bond is necessarily lengthened by this geometric distortion, while the remaining two C_α bond distances decrease. The perimeter C_β—C_β bond length is least affected, being shortened only slightly upon complex formation with Ni.

Table 1. Hartree-Fock (HF) energy (kcal/mol) relative to the C_{2v} minimum and HF e_u imaginary frequency (cm^{-1}) for the D_{4h} stationary point of NiP

Basis	Relative energy	Imaginary frequency
6-311G	0.002	i87
6-311G(d)	0.377	i799
GBS[a]	0.186	i657

[a] General basis set

4 Electronic structure and bonding

The electronic structure of NiP can be considered, to a first approximation, as arising from Ni^{+2} inserted into the P^{-2} complex. In this purely ionic description, i.e., crystal field theory, the Ni adopts a divalent d^8 electronic configuration, with the Ni 4*s* and $d_{x^2-y^2}$ orbitals formally empty. The occupation of the remaining 3*d* orbitals predicted by crystal field theory for D_{4h} symmetry is $(e_g)^4(a_{1g})^2(b_{2g})^2$. In metal coordination chemistry, the covalent contribution to the bonding mechanism can then enter as a σ donation from the porphyrin ligand (primarily through the nitrogens) into empty, low-lying Ni orbitals (i.e, the $d_{x^2-y^2}$ and 4*s* orbitals). The organometallic π back donation mechanism from metal d_π orbitals into ligand-centered p_{π^*} orbitals is less important in NiP given the Ni(II) oxidation state, although the porphyrin has acceptor character owing to its delocalized π network.

Table 3 lists Mulliken populations at the HF and MP2 levels of theory for the GBS basis. A Mulliken population analysis supports the importance of the ionic model at the HF level. The Ni population distribution and total charge of +1.5e is the same for all three basis sets. The 3*d* population is 8.1e with the individual valence orbital populations calculated as $d_{xy} = 2.0e$, $d_{xz} = d_{yz} = 2.0e$ each, $d_{z^2} = 1.9e$, $d_{x^2-y^2} = 0.2e$, and $4s = 0.3e$, with no significant population in the 4*p* orbitals. Some degree of σ donation into the Ni $d_{x^2-y^2}$ orbital is

Table 2. Selected optimized bond lengths (Å) and angles (degree) for NiP and P^{-2} in D_{4h} symmetry

Method	NiP					
	Ni—N	N—C_α	C_α—C_m	C_α—C_β	C_β—C_β	C_α—N—C_α
HF/6-311G	2.002	1.368	1.377	1.440	1.348	106.4
HF/6-311G(d)	1.998	1.354	1.380	1.438	1.344	106.2
HF/GBS[a]	1.999	1.356	1.380	1.438	1.350	106.2
MP2/GBS[a]	1.952	1.384	1.380	1.442	1.376	103.7
Experimental[b]	1.951	1.379	1.371	1.435	1.347	104.3
Method	P^{-2}					
	Ct—N[c]	N—C_α	C_α—C_m	C_α—C_β	C_β—C_β	C_α—N—C_α
HF/6-311G	2.086	1.346	1.397	1.469	1.354	108.8
HF/6-311G(d)	2.077	1.329	1.401	1.467	1.347	108.4
HF/GBS[a]	2.074	1.331	1.401	1.466	1.355	108.2
MP2/GBS[a]	2.073	1.362	1.411	1.469	1.388	106.7

[a] See text for description of the general basis set GBS
[b] Ref. [7] X-ray diffraction data
[c] Half of the distance between opposite Ns

Table 3. Mulliken population analysis for P^{-2} and NiP in D_{4h} symmetry at the HF/GBS[a] and MP2/GBS[a] levels of theory

	HF/GBS[a]			MP2/GBS[a]		
	P^{-2}	P^{-2}@NiP[b]	NiP	P^{-2}	P^{-2}@NiP[b]	NiP
Ni	–	–	1.5	–	–	1.2
N	−0.5	−0.5	−1.0	−0.4	−0.4	−0.7
C_α	0.2	0.2	0.3	0.1	0.1	0.1
C_β	−0.2	−0.2	−0.1	−0.1	−0.1	−0.1
C_m	−0.3	−0.3	−0.3	−0.3	−0.3	−0.2
H	0.1	0.1	0.2	0.1	0.1	0.2

[a] See text for description of the GBS
[b] P^{-2} fixed at the geometry of NiP

Table 4. Energy (a.u.) and character of pertinent D_{4h} orbitals of NiP at the HF/6-311G(d) level

Symmetry	Character	Orbital energy
b_{2g}	Pure $3d_{xy}$	−0.66
e_g	Primarily $3d_\pi$	−0.60
a_{1g}	Primarily $3d_{z^2}$	−0.57
a_{1g}	Nitrogen lone pair (σ donation to 4s and $3d_{z^2}$)	−0.50
b_{1g}	Nitrogen lone pair (σ donation to $3d_{x^2-y^2}$)	−0.47
a_{2u}	Ligand p_π (HOMO-1)	−0.25
a_{1u}	Ligand p_π (HOMO)	−0.22
e_g	Ligand $p_\pi{}^*$ (LUMO, LUMO + 1)	0.02

evident but π back-donation out of Ni d_π orbitals is not. Each nitrogen carries a significant negative charge of −1.0e, while the remaining charge is spread over slightly positive C_α and H atoms, and slightly negative C_β and C_m atoms. Since part of the Ni 4s population is likely owing to the diffuse nature of the highest s functions in the basis set, even more of the s population should be assigned to nitrogen.

The Mulliken population analysis at the MP2/GBS level favors a more covalent description of the Ni-porphyrin bonding, with the Ni charge reduced to +1.2e. The 3d population is increased to 8.3e with the individual valence orbital populations calculated as $d_{xy} = 1.9$e, $d_{xz} = d_{yz} = 2.0$e each, $d_{z^2} = 1.9$e, $d_{x^2-y^2} = 0.5$e, and $4s = 0.5$e, with no significant population in the 4p orbitals. A considerable increase in σ donation into the Ni $d_{x^2-y^2}$ orbital occurs when electron correlation is included, yet π back-donation is still not apparent. Each nitrogen carries a −0.7e charge which is less than the HF value. The remaining charge is spread over the rest of the atoms in a manner similar to the HF level.

To provide further insight into the metal-porphyrin interaction, a Mulliken population analysis was performed for P^{-2} at the HF and MP2 levels for the optimized D_{4h} geometries in Table 2. The calculation was repeated for p^{-2} fixed at the corresponding D_{4h} geometry of NiP (P^{-2}@NiP). Since the HF results are very similar for al three basis sets, only the HF/GBS populations are reported in Table 3, to facilitate comparison with the MP2/GBS results. At both the HF and MP2 levels, the slight distortion of the porphyrin framework to accommodate the central Ni results in negligible changes in the atomic charges between P^{-2} and P^{-2}@NiP. The most significant change between P^{-2}@NiP and NiP is the doubling of the negative charge on nitrogen in the latter. Rather than a consequence of d_π backbonding, this is due to small yet cumulative charge redistribution from the rest of the porphyrin framework onto the nitrogens.

The principal character and energies of the important orbitals of NiP are summarized in Table 4. Because of the similarities among all three basis sets, only the HF/6-311G(d) values are reported. In NiP, the energetic ordering of the Ni d orbitals is $(b_{2g})^2(e_g)^4(a_{1g})^2$. The dominant charge transfer is due to σ donation from ligand a_{1g} and b_{1g} orbitals that can be characterized as primarily nitrogen lone pairs into the formally empty Ni 4s and $d_{x^2-y^2}$. There is virtually no d_π backbonding into the ligand $e_g p_{\pi^*}$ orbitals.

Changes in the nitrogen bond lengths as function of complexation and correlation also contribute to interpreting the bonding mechanism. The magnitude of the bond-length changes from P^{-2} to NiP are approximately the same between the HF/GBS and MP2/GBS levels, except for the Ni—N bond. There is substantially more contraction of the core region upon NiP formation at the MP2/GBS level, i.e., 0.121 Å compared with 0.075 Å at the HF/GBS level, demonstrating increased covalent bonding with the inclusion of electron correlation. The N—C_α bond lengthening upon complexation is a geometric consequence of the core contraction, since the porphyrin framework is not that structurally flexible. The remaining bond-length changes from p^{-2} to NiP are due to the resulting charge redistribution throughout the ligand. The Ni—N bond-length shortening in NiP from the HF/GBS level to the MP2/GBS level is typical of correlation effects on metal-ligand bonds, and supports the increased role of covalent bonding (through σ donation) upon inclusion of correlation.

The electronic interpretation of porphyrin ground-state absorption and excited-state emission is historically described by the qualitative "four-orbital" model of Gouterman [8], which has been validated for H_2P at the CASPT2 level [2]. In this model, the first two molecular orbitals (MO) are occupied eight-node π MOs of a_{2u} and a_{1u} symmetry (HOMO-1, HOMO). There is a clear separation of the nearly degenerate HOMO and HOMO-1 from the rest of the occupied orbitals. The final two orbitals are a degenerate pair of empty ten-node π MOs of e_g symmetry (LUMO, LUMO+1), which are well-separated from the remaining virtual orbitals.

Within the four-orbital system, the HF orbitals for P^{-2} conform to the Gouterman model with one minor modification. There is not a large energy separation between the two HOMOs and the remaining filled orbitals. The corresponding four HF orbitals of NiP are very similar to those of P^{-2}; however, the HOMOs are now well separated from the remaining filled orbitals as in the Gouterman model. Small contributions also appear from the C_β—C_β π bonds to the a_{2u} HOMO and the e_g LUMOs.

There are tow previously published DFT studies [9, 10] of NiP, both of which give slightly differing views of

the electronic structure based on orbital character, ordering, and Mulliken population analysis. Of course, DFT Mulliken populations are based on orbital constituents of a density and not on orbitals corresponding to a determinantal wavefunction, and the basis set dependence of Mulliken populations precludes any detailed comparison to the results reported here. Both DFT investigations calculate a significantly smaller positive charge on Ni than either HF or MP2 do, but this is due in part to the differences in NiP geometries employed. Also, the DFT descriptions of the HOMO and LUMO consist of 3*d* orbitals as the primary components, and not the ligand p_π orbitals. In contrast, there is no *d* character in either the HOMO or the LUMO at the HF level or in the four-orbital Gouterman model. For comparative purposes, brief summaries of these DFT results follow.

In the first study, Rosa and Baerends [9] applied nonlocal DFT with a triple-zeta Slater basis set to a non-optimized NiP geometry, with an assumed Ni—N bond length of 1.96 Å. They find a Ni total charge of +0.6e, with a 3*d* population of 8.6e distributed as $d_{xy} = 2.0$e, $d_{xz} = d_{yz} = 1.9$e each, $d_{z^2} = 1.9$e, $d_{x^2-y^2} = 0.9$e, $4s = 0.4$e, and $4p = 0.4$e; (note that their paper employs a different axis convention). They conclude that the dominant bonding interaction is due to σ donation from nitrogen lone pairs into the $d_{x^2-y^2}$ orbital, with additional donation into the 4*s* and 4*p* orbitals. The total charge on each nitrogen is −0.6e. Back-donation from $3d_\pi$ to ligand p_{π^*} orbitals and donation from ligand p_π into Ni 4*p* orbitals are negligible. The HOMO is a Ni-centered combination of 4*s* and d_{z^2} orbitals, while the LUMO is a mixture of $d_{x^2-y^2}$ plus nitrogen lone pairs.

In the second study, Matsuzawa et al. [10] employed local DFT with a polarized double-numerical basis set. Their optimized Ni—N bond length of 1.935 Å is much shorter than the experimental X-ray value, but their remaining bond lengths are in more reasonable agreement. They find a Ni 3*d* population of 8.7e with the individual valence orbital populations calculated as $d_{xy} = 2.0$e, $d_{xz} = d_{yz} = 1.9$e each, $d_{z^2} = 1.9$e, $d_{x^2-y^2} = 1.0$e, $4s = 0.6$e, and $4p = 0.5$e. This results in a nearly neutral Ni with a total charge of +0.2e. Their HOMO is the degenerate d_π orbital and their LUMO is predominantly the $d_{x^2-y^2}$ orbital.

5 Harmonic frequencies

NiP in D_{4h} symmetry has 105 vibrational modes that transform as $9a_{1g}, 9b_{1g}, 8a_{2g}, 9b_{2g}, 18e_u, 3a_{1u}, 5b_{1u}, 6a_{2u}, 4b_{2u}$, and $8eg$ [11]. At the HF level, the D_{4h} structure of NiP has a degenerate pair of imaginary frequencies of e_u symmetry, which can subsequently affect the calculated values of the remaining e_u modes. However, modes of other symmetries should not be strongly affected. In fact, this was successfully demonstrated for H_2P [12], where HF/3-21G harmonic frequencies of the HF D_{2h} saddle point reproduced quite well the observed matrix infrared spectra. For NiP, the maximum difference between the non-e_u frequencies of the D_{h4} form and the corresponding frequencies of the C_{2v} minimum is only 3 cm^{-1} for the 6-311G basis set. For the GBS and 6-311G(d) basis set, the differences are greater due to the larger geometry changes and larger energy difference between the D_{4h} and C_{2v} structures, relative to those of the 6-311G basis. When there is a good correspondence between the nondegenerate modes of the D_{4h} and C_{2v} forms, the difference is in the order of 5–15 cm^{-1}.

Tables 5 and 6 present scaled HF/6-311G(d) frequencies in comparison to the results of three experimental studies. In the first of these, by Li et al. [13], solution-phase resonance Raman and infrared spectroscopies were used to identify 42 in-plane modes, 15 of which are of e_u symmetry. The spectra of three deuterated isotopomers of NiP were also measured. The mode labeling used herein is taken directly from this experimental work. A second resonance Raman study by Unger et al. [14] confirms the assignments of Li et al. for 15 modes. The most recent study by Jentzen et al. [7] applied resonance Raman spectroscopy to both single-crystal and solution forms, and confirms the assignments of six modes from the work of Li et al.

A scaling factor is typically applied to HF frequencies in order to correct for their systematic overestimation owing to the neglect of both electron correlation and anharmonic effects. A standard value of 0.89 [15] has been derived from fitting HF/6-311G(d) frequencies to empirical gas-phase data for molecules not containing transition metals. Since the comparison made here is to solution data, it is reasonable to modify this standard scaling factor to account for solvent effects as well as for the use of the larger 6-311G(d) basis. The best fit to the data of Li et al. [13] is achieved with a uniform scale factor of 0.91.

From Tables 5 and 6, it can be seen that the resulting deviations from the observed fundamentals [13] are typically under 15 cm^{-1}, with a few in the range of 20 cm^{-1}. The largest differences occur for the lowest b_{2g} mode and the highest a_{2g} mode, with an error near 30 cm^{-1}. The HF/6-311G(d) normal coordinates conform qualitatively with the local coordinate description of Li et al. [13] derived from valence force field calculations. This agreement is strong evidence that the in-plane normal modes of NiP are well understood. Li et al. also assigned 15 in-plane e_u modes, but the use of D_{4h} frequencies precludes comparison to the scaled HF values, for the reason discussed above. Apart from the imaginary e_u mode which correlates with in-plane N—C_α, C_α—C_m, and C_α—C_β stretching toward the bond-alternating C_{2v} geometry, however, the agreement with the remaining observed e_u modes is actually quite satisfactory.

Isotopic frequencies were computed for NiP with deuteriums replacing hydrogens bonded to the C_α, C_β, and C_α + C_β carbons (labeled NiP-d_4, d_8, and d_{12}, respectively), and then scaled uniformly by 0.91. The results for these isotopomers are listed in Tables 5 and 6, and the experimental isotope effects are well reproduced. The average magnitude of the deviation from the observed fundamentals is 17 cm^{-1}. There are a few instances where the disagreement is much larger, but the only egregious one is the 75 cm^{-1} difference for the ν_{26} mode in NiP-d_{12}. In this case, the experimental band at 848 cm^{-1} is attributed to both the a_{2g} mode ν_{26} and the

Table 5. Scaled[a] a_{1g} and b_{1g} HF/6-311G(d) frequencies (cm^{-1}) for the D_{4h} structure of NiP, with corresponding observed fundamentals for NiP[b,c,d] and its isotopomers[b]

	NiP				NiP-d_4		NiP-d_8		NiP-d_{12}	
	HF[a]	Expt.[b]	Expt.[c]	Expt.[d]	HF[a]	Expt.[b]	HF[a]	Expt.[b]	HF[a]	Expt.[b]
a_{1g}										
ν_5	3104	–	–	–	3103	–	2318	–	2318	–
ν_1	3061	–	–	–	2263	–	3061	–	2263	–
ν_2	1587	1574	1572	1575; 1576	1581	1566	1559	1552	1550	1546
ν_3	1465	1459	–	–	1458	1456	1442	1431	1439	1427
ν_4	1390	1376	1376	1377;1378	1390	1374	1379	1367	1379	1367
ν_9	1075	1066	1065	–	1075	1065	778	775	777	773
ν_6	995	995	994	–	992	992	986	987	985	985
ν_7	725	732	–	–	703	711	722	720	701	709
ν_8	351	369	–	–	350	367	344	360	343	359
b_{1g}										
ν_{14}	3103	–	–	–	3103	–	2317	–	2317	–
ν_{10}	1628	1650	1648	1651; 1651	1613	1642	1625	1646	1609	1636
ν_{11}	1525	1505	1502	–	1522	1504	1471	1454	1465	1454
ν_{12}	1408	–	–	–	1344	1321	1405	1324	1344	1315
ν_{13}	1198	1185	1184	–	958	938	1193	1179	964	948
ν_{17}	1067	1060	1058	–	1087	–	803	768	773	768
ν_{15}	997	1003	1002	–	1007	1020	981	–	1012	–
ν_{16}	734	732	–	–	668	665	707	705	661	655
ν_{18}	216	237	–	–	216	237	212	232	212	232

[a] Scaled by 0.91; see text for details
[b] Ref. [13] infrared and resonance Raman solution data
[c] Ref. [14] resonance Raman solution data
[d] Ref. [7] first value from resonance Raman single-crystal data and second value from resonance Raman solution data

Table 6. Scaled[a] a_{2g} and b_{2g} HF/6-311G(d) frequencies (cm^{-1}) for the D_{4h} structure of NiP, with corresponding observed fundamentals for NiP[b,c,d] and its isotopomers[b]

	NiP				NiP-d_4		NiP-d_8		NiP-d_{12}	
	HF[a]	Expt.[b]	Expt.[c]	Expt.[d]	HF[a]	Expt.[b]	HF[a]	Expt.[b]	HF[a]	Expt.[b]
a_{2g}										
ν_{23}	3083	–	–	–	3083	–	2278	–	2278	–
ν_{19}	1582	1611	1603	1608; 1606	1557	1598	1579	1605	1551	1592
ν_{20}	1371	1354	–	–	1358	1347	1331	1313	1298	1278
ν_{26}	1331	1317	1315	1317; 1317	1284	1249	854	851	923	848
ν_{21}	1162	1139	1137	–	925	910	1265	1256	847	848
ν_{22}	1006	1005	1003	–	1010	1012	1118	1095	1204	1189
ν_{24}	796	806	–	–	775	783	777	788	761	767
ν_{25}	420	429	–	–	410	419	398	404	389	397
b_{2g}										
ν_{31}	3083	–	–	–	3083	–	2278	–	2279	–
ν_{27}	3060	–	–	–	2262	–	3061	–	2261	–
ν_{28}	1502	1505	–	–	1497	1477	1482	1487	1475	1481
ν_{29}	1383	1368	1354	1355; 1356	1380	1368	1343	1324	1343	1315
ν_{34}	1198	1193	1193	–	1197	1193	971	–	965	948
ν_{30}	1063	–	–	–	1047	1020	1086	–	1072	–
ν_{32}	824	819	–	–	814	815	770	799	764	780
ν_{33}	415	435	–	–	415	432	381	399	381	399
ν_{35}	228	197	–	–	224	197	226	197	223	197

[a] Scaled by 0.91; see text for details
[b] Ref. [13] infrared and resonance Raman solution data
[c] Ref. [14] resonance Raman solution data
[d] Ref. [7] first value from resonance Raman single-crystal data and second value from resonance Raman solution data

a_{2g} mode ν_{21}. This assignment seems rather unlikely based on the present HF results.

The remaining modes of $a_{1u}, b_{1u}, a_{2u}, b_{2u}$, and e_g symmetry correspond to out-of-plane distortions categorized [16] as propeller (pro), ruffle (ruf), dome (dom), saddle (sad), and wave (wav), respectively (Table 7). The lowest modes of each symmetry can be described as follows. The a_{1u} propeller mode has each pyrrole ring twisted in the same direction about its Ni—N bond. The b_{1u} ruffling mode is similar to the propeller motion but

Table 7. Scaled[a] HF/6-311G(d) frequencies (cm^{-1}) for the D_{4h} structure of NiP, for symmetries a_{1u}, b_{1u}, a_{2u}, and e_g. The out-of-plane distortions are categorized as propeller (pro), ruffle (ruf), dome (dom), saddle (sad), and wave (wav)

a_{1u} (pro)	b_{1u} (ruf)	a_{2u} (dom)	b_{2u} (sad)	e_g (wav)
938	944	885	816	942
688	864	797	682	875
289	703	729	249	805
	474	355	52	718
	52	257		678
		93		434
				216
				152

[a] Scaled by 0.91, see text for details

with alternate pyrrole rings twisted in opposite directions about their Ni—N bonds. The a_{2u} doming mode has the central Ni and the nitrogens pulled up from the mean plane of the porphyrin framework, with the beta carbons pulled down. The b_{2u} saddling mode consists of alternate pyrrole rings displaced up or down while the meso carbons remain in the mean plane. The degenerate e_g waving mode has one pair of opposing pyrrole rings displaced up and down, while the other pair are twisted in the same direction about their Ni—N bonds.

The out-of-plane vibrations that are either IR or Raman active have not yet been experimentally measured. Table 7 reports scaled HF/6-311G(d) values for these frequencies, which are sensitive to nonplanar conformations in substituted nickel porphyrins where steric interactions induce a variety of types and degrees of nonplanarity. The results in Table 7 will therefore be relevant to future theoretical studies that examine substituent effects in metalloporphyrins. For larger functionalized nickel porphyrins, of course, HF harmonic frequency determinations are feasible only with smaller basis sets.

6 Summary

The HF description of NiP suffers from a symmetry-breaking artifact, albeit with a very low energy difference of 0.4 kcal/mol between the C_{2v} minimum and the localized D_{4h}-stationary point. The D_{4h} geometry is in satisfactory agreement with a recent crystal structure determination, i.e., within the expected degree of accuracy for transition metal-ligand bonding at the HF level. Accounting for electron correlation effects at the MP2 level considerably improves the agreement with experiment.

The Ni $d_{x^2-y^2}$ orbital, which is formally empty in an ionic description of the bonding, is moderately populated at the HF level due to σ donation from nitrogen lone pairs on the ligand. However, the HF description of the Ni-porphyrin interaction remains rather ionic. With the inclusion of correlation at the MP2 level, σ donation is notably enhanced and is the dominant bonding mechanism. There is little evidence fof π backbonding at either the HF of MP2 levels. The historical "four-orbital" model of Gouterman is validated for NiP and the dianion P^{-2}. The HOMOs and LUMOs consist of ligand p_π-centered orbitals, in contrast to earlier DFT predictions of considerable Ni $3d$ character in these orbitals.

Harmonic frequencies computed at the HF level and uniformly scaled compare quite well with observed in-plane IR and resonance Raman data of NiP and its isotopomers. This satisfactory level of agreement suggests that scaled HF frequencies may be adequate for nickel porphyrins with large substituent groups. Frequencies are also reported for out-of-plane vibrations, as these will provide the key in future studies of substituted nickel porphyrins, where multiple nonplanar conformations are possible.

Acknowledgements. This work was supported by the Laboratory-Directed Research and Development Program of Sandia National Laboratories, under contract with the U.S. Department of Energy, and by the University of Minnesota Supercomputer Institute. M.C.P. thanks M.E.C. for a grant. The authors thank Prof. Peter Pulay, Dr. Pawel Kozlowski, Mr. Andrzej Jarzecki, and Prof. Vincent Ortiz for helpful discussions. The authors also acknowledge the expert guidance provided by the late Prof. Jan Almlöf in the initial stages of this research.

References

1. Almlöf JE, Fischer TH, Gassman PG, Ghosh A, Häser M, (1993) J Phys Chem 97: 10964
2. Merchan M, Orti E, Roos BO, (1994) Chem Phys Lett 221: 136
3. Kozlowski PM, Zgierski MZ, Pulay P (1995) Chem Phys Lett 247: 379; Kozlowski PM, Jarzecki AA, Pulay P (1996) J Phys Chem 100: 7007; Kozlowski PM, Jarzecki AA, Pulay P, Li X -Y, Zgierski MZ (1996) J Phys Chem 100: 13985
4. Pulay P, Kozlowski PM (private communication)
5. Piqueras MC, Rohlfing CM (1996) J Mol Struct 388: 293
6. Frisch MJ, Trucks GW, Schlegel HB, Gill PMW, Johnson BG Robb MA, Cheeseman JR, Keith T, Petersson GA, Montgomery JA, Raghavachari K, Al-Laham MA, Zakrzewski VG, Ortiz JV, Foresman JB, Cioslowski J, Stefanoy BB, Nanayakkara A, Challacombe M, Peng CY, Ayala PY, Chen W, Wong MW, Andres JL, Replogle ES, Gomperts R, Martin RL, Fox DJ, Binkley JS, Defrees DJ, Baker J, Stewart JP, Head-Gordon M, Gonzalez C, Pople JA (1995) Gaussian 94. Gaussian Inc., Pittsburgh, Pa
7. Jentzen W, Turowska-Tyrk I, Scheidt WR, Shelnutt JA (1996) Inorg Chem 35: 3559
8. Gouterman M (1978) In: Dolphin D (ed) The porphyrins, vol III. Academic Press, New York, p 1
9. Rosa A, Baerends EJ (1994) Inorg Chem 33: 584
10. Matsuzawa N, Ata M, Dixon DA (1995) J Phys Chem 99: 7698
11. Procyk AD, Bocian DF (1992) Ann Rev Phys Chem 43: 465
12. Radzisewski JG, Nepras M, Balaji V, Waluk J, Vogel E, Michl J (1995) Phys Chem 99: 14254
13. Li X-Y, Czernuszewicz RS, Kincaid JR, Su YO, Spiro TG (1990) J Phys chem 94: 31
14. Unger E, Bobinger U, Dreybrodt W, Schweitzer-Stenner R (1993) J Phys Chem 97: 9956
15. Pople, JA, Head-Gordon M, Fox DJ, Raghavachari K, Curtiss LA (1989) J Chem Phys 90: 5622
16. Scheidt WR, Lee YJ (1987) In: Structure and bonding, vol 64. Springer Berlin, Heidelberg New York p 2